THE TAROT SUSPECTED VARIABLE STAR CATALOG[1]

Y. DAMERDJI,[2,3] A. KLOTZ,[2,3] AND M. BOËR[3]

ABSTRACT

TAROT (Télescope à Action Rapide pour les Objets Transitoires) is a robotic observatory designed to observe very early optical transients of gamma-ray bursts (GRBs). As GRBs do not often occur, we use TAROT for various other celestial targets spread over the sky. For every field observed by TAROT, we computed the magnitudes of every star. From this work, we found 1175 new variable stars brighter than 17 mag. We selected the best variable star candidates and compiled them in the TSVSC1 (TAROT Suspected Variable Star Catalog, ver. 1), which also contains Fourier-series coefficients that fit the light curves.

Key words: stars: variables: other — techniques: photometric

Online material: color figure, tar file

1. INTRODUCTION

Variability of stars helps to increase our knowledge about processes that govern stellar physics. Accurate studies of some of the brightest stars of each type of variability have been performed since they were discovered. However, large statistical studies on the variability classes can help to solve fundamental problems such as the initial mass function.

Traditionally, discoveries of variable stars are compiled in the General Catalog of Variable Stars (GCVS). The GCVS, version 4.2, contains 38,624 designated variable stars (Samus et al. 2004). There are no light curves—only periods, amplitudes, and types when known. The New Suspected Variable (NSV) catalog is an extension with 26,017 additional variable candidates. These catalogs do not allow us to perform statistical studies without strong biases due to the heterogeneity of the input data.

Since the end of the 20th century, many wide-field optics have been equipped with large CCDs. Bidimensional analysis is much more powerful than single-channel photometers or eye examination for discovering new variables. Moreover, robotic telescopes can optimize observation strategies without human intervention at night.

The first large all-sky survey to detect variables was carried out by Wozniak et al. (2004) with the ROTSE-I telescope. They produced the Northern Sky Variability Survey (NSVS), and light curves can be downloaded via the SkyDOT Web site. The survey was conducted over 1 year of observations using four telelenses, with $f = 200$ mm, $f/D = 1.8$, and a sampling of $14''$ pixel^{-1}. The field of view is $8° \times 8°$ for each optic. The magnitude range is 11–15. About 5×10^5 stars were found to be variable at a limit of ± 0.05 mag among 14×10^6 stars; hence, 3.5% of stars exhibit amplitudes higher than 0.05 mag. A total of 30,000 deg^2 were scanned.

The All Sky Automated Survey (ASAS; Pojmański 2002) has evolved continuously since 1997. The actual ASAS-3 system consists of four optics: one $f = 750$ mm, $f/D = 3$ instrument, two $f = 200$ mm, $f/D = 2.8$ instruments, and one $f = 50$ mm, $f/D = 4$ instrument. The magnitudes studied are brighter than 13. Since 1997, ASAS-1 has observed 300 deg^2, and 140,000 stars have been measured multiple times. A total of 3900 stars were found to have variability higher than 0.1 mag rms; among them 10% were recognized as periodic variables. From the ASAS study, 2.7% of stars are detected to have variability higher than 0.1 mag.

Other large surveys have also been conducted. Microlensing detection programs have allowed the establishment of deep surveys in small areas. The Optical Gravitational Lensing Experiment (OGLE) has been performed using the 1.3 m Warsaw Telescope (Udalski et al. 1994). Selected fields, covering about 100 deg^2, have been observed very regularly to follow up star variabilities. A real-time detection system of transient objects and catalogs for OGLE variable stars are available online.

TAROT (Télescope à Action Rapide pour les Objets Transitoires) is a robotic observatory designed for gamma-ray burst (GRB) detections (e.g., Bringer et al. 1999; Klotz et al. 2005). TAROT is also used for many other studies (see § 2). Every image taken by TAROT since 2004 January is photometrically analyzed in order to detect variable stars. This paper presents results of the first 30 months of observations. The list containing characteristics of these variable stars is designated TSVSC1 (TAROT Suspected Variable Star Catalog, ver. 1).

2. OBSERVATIONS

TAROT is a robotic observatory located at the Calern Observatory (43.7522° latitude north, 6.92389° longitude east, 1270 m altitude). The telescope diameter is 25 cm, and the focal length is 85 cm. Optical quality is achieved by an optical doublet corrector placed at the Newtonian focus. A filter wheel allows us to acquire images through standard *B*, *V*, *R*, and *I* photometric bands. An additional position (hereafter referred to as the *C* filter) is provided by a neutral glass filter (Schott WG280).

Before 2004 March 20, we used a custom camera based on a TH7899M chip (hereafter CAM1). Since 2004 March 20, we have been using an Andor Marconi 4240 camera (hereafter CAM2). Table 1 shows the main characteristics of CAM2 coupled

---

[2] CESR CNRS-UPS, Toulouse, France; klotz@cesr.fr.
[3] Observatoire de Haute-Provence, Saint Michel de Provence, France; damerdji@obs-hp.fr, boer@obs-hp.fr.

TABLE 1
TAROT Characteristic Setup with CAM2, Used since 2004 March 20

Quantity	Value
Mirror diameter...	25 cm
Field of view...	$1.86° \times 1.86°$
CCD	Marconi 42-40, thin back-illuminated
Number of pixels	2048×2048
Pixel size..	13.5 μm
Angular sampling..	3.3″
Readout time..	5 s
Readout noise..	8.5 e^-
Filter wheel	BVRIC
Limiting magnitude with C filter in 10 s....................	$V \sim 16.2$ at 3 σ
Limiting magnitude with C filter in 1 minute	$V \sim 18.2$ at 3 σ
Routine integration time	10–100 s
Flat fields	Artificial only

to TAROT. The CAM1 characteristics are almost the same, except that the CCD is thick front-illuminated, the pixel size is 14 μm, and the readout noise is 13 e^-.

The main goal of TAROT is to observe GRB fields, but this is less than 5% of the total time. Aside from GRBs, TAROT is used to record images but is not devoted to a large sky survey as done by ROTSE or by ASAS. The telescope is used to observe specific targets: photometry of minor planets such as near-Earth asteroids (e.g., Pravec et al. 2003), binary minor planets (e.g., Behrend et al. 2006), star occultations by minor planets,[4] follow-up of selected RR Lyrae stars (e.g., Le Borgne 2004), searches for supernovae (e.g., Zwitter et al. 2004), and other targets of opportunity.

This paper shows the results obtained by a systematic photometric analysis of each image taken by TAROT between 2004 January and 2006 June. Obviously, the scheduling strategy, based on selected targets, induces strong biases in the statistical interpretations of the new variable sources detected. As a consequence, the TSVSC1 is not an all-sky survey of variable stars. Only a few fields are observed (see Fig. 1), allowing us to find the largest possible range of periodic variables.

A follow-up of some variable-star candidates of the TSVSC1 was done using the 80 cm telescope at the Observatoire de Haute-Provence, France. These observations were used to validate the limits of the algorithms used to extract the variable stars of the TSVSC1.

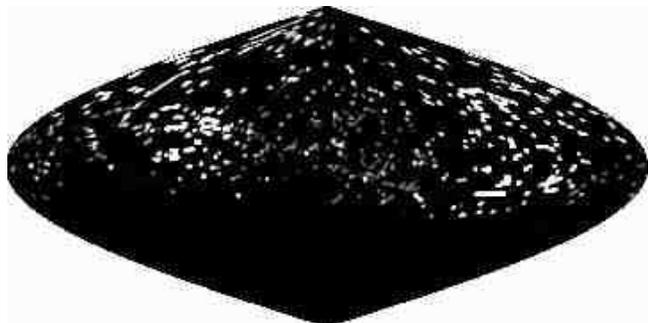[4] The Web site http://www.euraster.net provides information on these occultations.

Fig. 1.—Sanson-Flamsteed sky projection of the TAROT observed fields reported in the equatorial frame. Brightness is proportional to the number of stars recorded. Twelve percent of the sky observable from Calern Observatory was recorded at least one time by TAROT.

3. DATA REDUCTIONS

3.1. Star Magnitude Measurements

Raw images are processed by classical dark subtraction followed by flat-field division. A background image (for scales higher than 3′) is synthesized and then subtracted to eliminate residual lunar reflections that appear sometimes due to the Newtonian setup. A smooth median filter was used to clip cosmic-ray pixels until 2005 November. Flux measurements are performed with SExtractor (Bertin & Arnouts 1996). Then an astrometric calibration of the entire field is performed using the USNO-A2.0 catalog. This is also used for the determination of the zero point of the magnitudes using the R magnitudes of the catalog. As a consequence of this method, the TSVSC1 magnitudes are not linked directly to standard colors. However, differential photometry is possible. This latter method is used to extract variable stars.

Each star measured is recorded in a large database in which the sky is sliced into a hierarchical triangular mesh (HTM) of eighth level (Kunszt et al. 2001). At this level, an HTM area spreads about 280 arcmin^2. In each area, stars are matched by their celestial coordinates and are indexed by an integer number, incremented as a new star is appended in the database. For instance, the star TN-N002320222-31 has the index 31 in the area N002320222 defined by Kunszt et al. (2001). The TN acronym designates TAROT North. Another catalog will be set up later from the data of the TAROT South telescope, described in Boër et al. (2003).

In an HTM area, each star can be described as a series of Julian day, magnitude, magnitude error, and flag given by SExtractor. Magnitude on a given date is not related to an absolute reference-star field. As a consequence, a nonvariable star can exhibit variations in the database due to sky transparency variation. However, other nonvariable stars of the HTM area should exhibit the same variations. The differential photometry consists of computing a magnitude offset for each date and applying it to all star magnitudes. In this paper, we use the term corrected magnitude for the magnitude that includes these offsets. Offsets are calculated to minimize temporal variations. Obviously, true variable stars disturb the offset values, but they are eliminated by using a median criterion. At the end of the process, variations of the corrected magnitudes can be interpreted as intrinsic variations from the star. Note that we do not take into account the differential color index variations that can appear from various air mass measurements. This limits the accuracy to about ±0.05 mag. Moreover, other erratic magnitude variations can occur due to nonphotometric conditions of observation, blendings, or saturations.

3.2. Variable-Star Extraction

Variable stars are automatically identified using the technique described in Stetson (1996). This technique is more sensitive to intrinsic variations than the magnitude–standard deviation comparison (e.g., Pojmański 2002). Indeed, by pairing successive observations, false measurements are easily identified and their contributions in the variability index are diminished. Most of the TAROT observations are paired observations, done with either the same filter or a different one. Measurements are gathered within 10 minutes, since the star magnitude variation in this span is close to the measurement uncertainty (this means that tested periods must be much greater than this interval; see § 4.1). If x observations belong to the same span, individual measurement is included in $x - 1$ pairs, and each pair is weighted by $2/x$. Single measurements are half-weighted to avoid their large contributions if they are corrupted. The variability index is

$$L = JK/0.798, \qquad (1)$$

where K is the kurtosis of the magnitude histogram,

$$K = \frac{\sum_{i=1}^{N} |\delta_i|}{\sqrt{N \sum_{i=1}^{N} \delta_i^2}}. \qquad (2)$$

N denotes the total number of observations, and δ_i is the measurement residual from the mean:

$$\delta_i = \sqrt{\frac{N_j}{N_j - 1}} \frac{m_{ij} - \overline{m_j}}{\Delta m_{ij}}, \qquad (3)$$

where N_j is the number of measurements in the filter j, $\overline{m_j}$ is the weighted mean of Stetson (1996), and Δm_{ij} is the photometric error calculated by SExtractor. Also,

$$J = \frac{\sum_{k=1}^{n} w_k \, \text{sgn}(P_k) \sqrt{|P_k|}}{\sum_{k=1}^{n} w_k}, \qquad (4)$$

where n is the number of pairs (a pair may contain one observation), w_k is the pair weight, and

$$P_k = \begin{cases} \delta_{i(k)} \delta_{j(k)}, & i(k) \neq j(k), \\ \delta_{i(k)}^2 - 1, & i(k) = j(k). \end{cases} \qquad (5)$$

Variable star candidates are such that their variability index $L > 2$ (see Fig. 2). For the moment, this threshold does not depend on magnitude or air mass to favor brighter variable stars. The star must be measured at least 30 times, and the total amplitude must be higher than 0.1 mag. When a star is identified as a variable candidate, a text file is created containing its coordinates and a list of the topocentric Julian day, corrected magnitude, error in the magnitude, and SExtractor flag. Extracted variable candidates include many nonvariable stars polluted by some false measurements due to airplane or satellite tracks or cloudy variations. The next sections are devoted to the extraction of a subset of stars that exhibit variations compatible with intrinsic star variations.
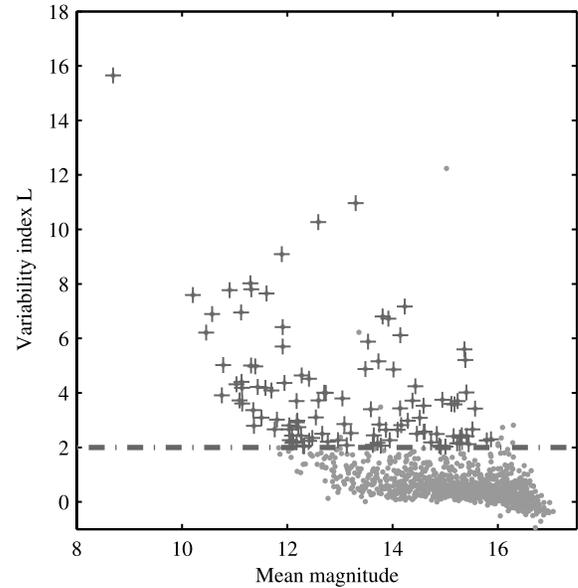

FIG. 2.—TAROT variability index L of the HTM area N032123222. This area was observed as a series of 30 s integrations between the Julian days 2,453,154.476 and 2,453,275.664. Extracted variable stars, represented by crosses, are above the threshold line and must have at least 30 measurements.

4. VARIABLE-CANDIDATE ANALYSIS

About 45% of the GCVS, version 4.2, variable stars have known periods. This leads us to look for periodicity in magnitude variations for each extracted star. We use many methods (see § 4.1) to determine the period, and therefore light-curve characteristics (period, Fourier-series coefficients for the folded light curve, classification, etc.), as quickly as possible. About 15% of the variable stars we extracted are compatible with periodic variations. For these stars, a synthetic folded light curve (FLC) is fitted by a Fourier-series expansion. The software implementation of the methods was done using Tcl/Tk scripts in the AudeLA software.[5]

4.1. Period Determination

Since there are many users observing on the same night with TAROT, variable-star data sets do not contain more than a few points per night. Some fields are frequently observed, whereas others are reobserved only by chance. To extract periodicity from this kind of irregularly spaced data, specific methods have been developed, since the standard methods, such as the Fourier transform, are unusable. Some of these methods are based on the fact that the FLC is smoothest when it is visualized within its real period. They transform the set of data by folding within the phase interval $0 \leq \varphi < 1$ defined by

$$\varphi(i) = \frac{t(i) - t_0}{P} - E\left(\frac{t(i) - t_0}{P}\right), \qquad (6)$$

where dates $t(i)$ are converted into the solar system barycentric frame, t_0 is the time origin, P is a test period, and E denotes the integer function. Because of the observational gaps, computed phases can have the same result for several test periods. These periods, often related, are aliases (see § 4.1.1). We separated

---

[5] See http://audela.ccdaude.com.

the best period P_{best} from its aliases using several methods (see §§ 4.1.2–4.1.4).

4.1.1. Period Selection

Given a series of N observations, we define D_0, the pseudo–greatest common divisor of successive date differences as described by Eyer & Bartholdi (1999), and T, the total time range of observations. The shortest period to try is $P_0 = 2D_0$. Sometimes two or more frames are shot successively, leading to an unphysical P_0 value. To avoid this, we take P_0 as the greater of 0.04 day and $2D_0$; P_{max}, the largest period to test, is taken to be equal to $2T$, in order to treat as periodic those stars that show only a part of their variation during the range of observation (useful for identifying long-period variables and nova candidates). However, in the final selection, we select only variables having periods that satisfy $P < T/2$. The period step is taken as described in Akerlof et al. (1994) and Larsson (1996),

$$\Delta P = \sqrt{\frac{6}{N}} \frac{\sigma P^2}{\pi TA}, \qquad (7)$$

where A and σ are the amplitude and the noise of the signal, respectively.

Many periods are spurious because they correspond to many gaps in the data set (daytime, seasons, etc.). If P is the true period, and P_{gaps} is the period of gaps, spurious periods are given by

$$P_{\text{spur}}^{-1} = P^{-1} \pm k P_{\text{gaps}}^{-1}, \qquad (8)$$

where $k \in \mathcal{N}$.

4.1.2. Searching for the 100 Best Periods

Figure 3 shows that the spectrum of the residual χ^2 is very complex. No method leads inevitably to the true period in any case (rank is generally smaller than 20th but not necessarily the first). Each statistic criterion depends on the layout of points in phase-magnitude space, in which each point has its own behavior. Hence, the true period cannot be carried out by a dichotomy treatment due to the sharp peaks, as can be seen in Figure 3 (top).

Long-period variable star spectra are dominated by spurious periods related to the 1 day period gap (see Fig. 3). We use the method of phase-dispersion minimization (PDM) to identify whether the variable presents long- or short-term variations. We compare the deepest peak for long periods with the deepest one in the neighborhood of 1 and 0.5 days. This method consists of dividing the phase interval into n equal bins and calculating magnitude dispersion for each of them. Their sum is the smallest when data are folded over the true period. As described in Stellingwerf (1978) accuracy is better with increased n, but the efficiency decreases when $n > N/5$. Therefore, we use $n = \min(16, N/10)$ for long-term variables and $n = \min(8, N/10)$ for the rest.

Using the PDM method, we extract the 100 best periods among the thousands given in § 4.1.1. However, when the star presents short-term variations, the number of periods given by equation (7) can be very high. We reduce it by selecting an interval T' in T (with N' measurements and an amplitude A') having approximately 10^5 periods to test. The interval T' has the greatest $A'N'^2$.

4.1.3. Searching for the 10 Best Periods

We use additional methods to increase separation constraints in order to select the 10 best periods among the 100 selected in § 4.1.2. To do this, we compute the criteria of three methods.
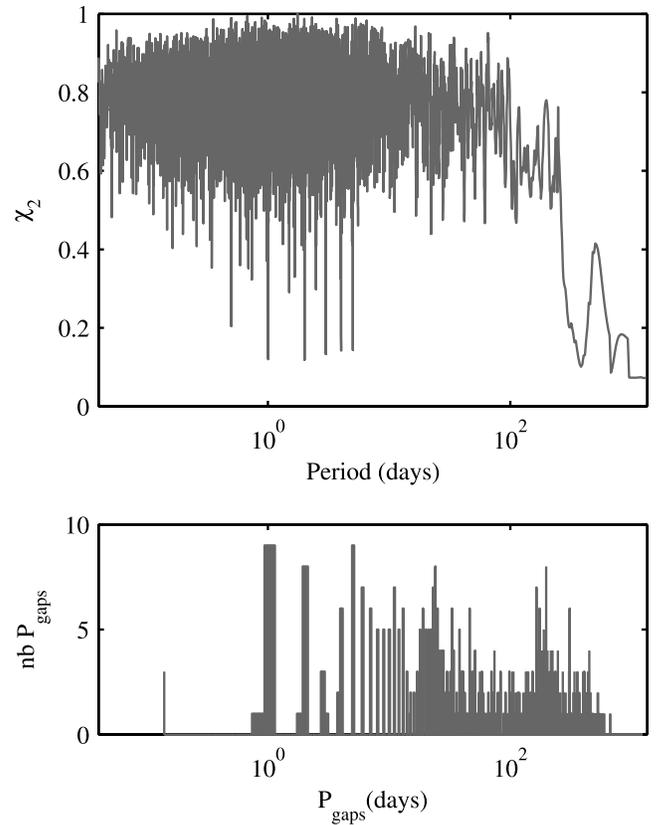

Fig. 3.—*Top*: Normalized residual χ^2 of T Cam (a Mira variable with a period of 373.2 days, corresponding to TAROT variable TN-N313121331-272-67-2). The TAROT data contain 667 days of observations ($D_{\text{max}} = 1334$ days) and $P_{\text{best}} = 371.79$ days. Spurious periods of 0.5, 1, 2, 3, 4, and 5 days, related to the gap of 1 day, have significant peaks in this spectrum. *Bottom*: Histogram of corresponding P_{gaps} allowing us to identify aliasing periods (highest peaks).

The string-length minimization (SLM) method was developed first by Lafler & Kinman (1965) and improved by Stetson (1996). The true period minimizes the value of

$$\Theta = \frac{\sum_{i=1}^{N-1} w_{i,i+1} |m_{i+1} - m_i|}{\sum_{i=1}^{N-1} w_{i,i+1}}, \qquad (9)$$

where

$$w_{i,i+1} = \frac{1}{(\Delta m_{i+1}^2 + \Delta m_i^2)(\varphi_{i+1} - \varphi_i + \epsilon)}, \qquad (10)$$

and φ_i, m_i, and Δm_i are phases, magnitudes, and magnitude uncertainties, respectively, sorted in order of increasing phase. The variable ε is a term added to diminish the weight of very short gaps in the phase interval. The PDM criterion is identical to the Lafler & Kinman (1965) one if each bin contains two observations.

Entropy minimization is the second method. Developed by Cincotta et al. (1995), it is based on the fact that data in phase-magnitude space are more ordered when phases are determined using the true period. Phase-magnitude space is divided into $n \times m$ bins. If we denote a_{ij} as the number of observations in the (i, j) bin normalized by the total number of data, the entropy S is

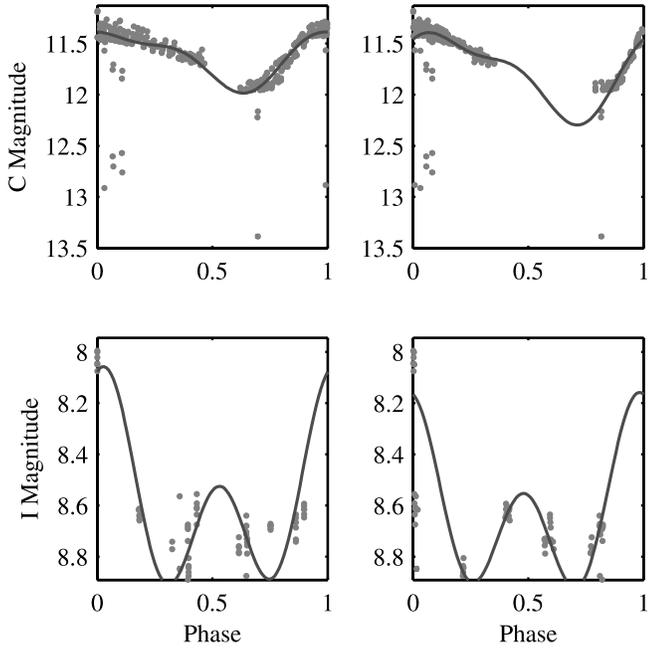$$S = \sum_{i=1}^{n} \sum_{j=1}^{m} a_{ij} \ln(a_{ij}) \forall a_{ij} > 0. \qquad (11)$$

Fig. 4.—*Top*: RW Cnc variable corresponding to TN-N233022110-29-67-2. In the top left panel FLC is carried out with $P_{best} = 0.353343$ days, whereas in the top right panel it is folded with the true period $P_{GCVS} = 0.547199$ days. Here, the large gap in the phase is responsible for the period-determination failure. *Bottom*: IM Aur variable corresponding to TN-N332032302-12-73-2. In the bottom left panel FLC is carried out with $P_{best} = 27.87392$ days. In the bottom right panel it is folded with the true period $P_{GCVS} = 1.247296$ days. Here, the period-determination failure is due to the bad sampling and some bad measurements.

We compute the periodogram as defined by Scargle (1982) only for long-period variables, since this criterion is not very efficient when the number of measurements per period becomes small.

For each of these three methods plus the PDM described in § 4.1.2, we compute the rank for each of the 100 best periods previously selected. The best periods should be those that verify the lowest rank for the four methods. To perform that, we compute the superrank as the sum of the ranks of the four methods. We select the 10 best periods as the 10 lowest superrank values.

4.1.4. Searching for the Best Period

In order to select the best period among the 10 selected in § 4.1.3, we use the χ^2 test, in which Fourier coefficients $a_0, (a_i, b_i)$ fit the data in the following equation:

$$m(i) = a_0 + \sum_{k=1}^{K} a_k \cos[2k\pi\varphi(i)] + b_k \sin[2k\pi\varphi(i)], \quad (12)$$

where K is adapted to the width of the largest gap in the phase of FLC (at most $K = 5$) and $\varphi(i)$ is calculated using equation (6).

At the end of the treatment, light curves are visualized, manually checked, and added to the TSVSC1 when they seem to have real variations; see Figure 4 for an example. For some long-period variables, our method converges to the multiple of the period, since there are some changes in the shape of the light curve from one period to another. We manually corrected P_{best} by selecting new values for P_0 and P_{max}. We also use this tool to fold over the double-period light curves showing eclipsing star–like variations.
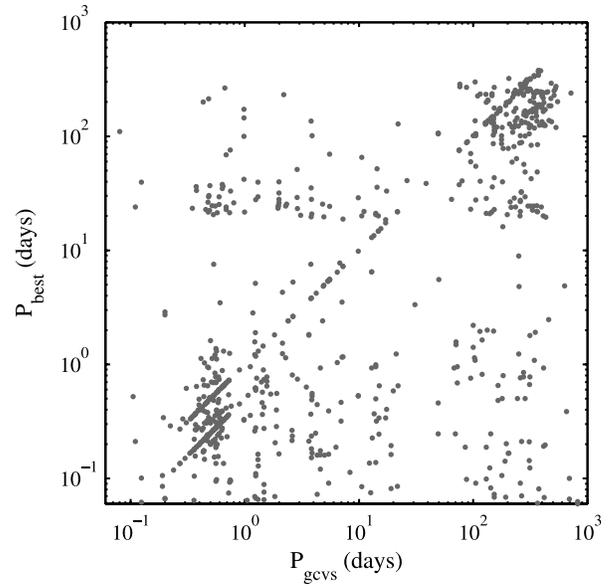

Fig. 5.—P_{GCVS} against P_{best} for 875 GCVS variables observed by TAROT.

Some dubious short-period variable stars were followed up with the 80 cm aperture telescope at the Observatoire de Haute-Provence to confirm their variations.

4.1.5. Comparisons with Known Variables of the GCVS

We find 875 variables known in the GCVS for which we are able to determine the period in TAROT data using the algorithm described earlier (the P_{GCVS} period is in the range of $[P_0, T/2]$). We find another 377 ROTSE and 650 ASAS variables, but we do not include them in this statistic since their periods are globally less accurate. Figure 5 shows that many P_{best} are equal to $0.5P_{GCVS}$. This artifact is related to the TAROT scientific program meant to measure the Blazhko effect of a hundred or so RR Lyrae stars: it observes only near maximum light, so only a part of the light curve is available. The period-determination failure for P_{GCVS} close to 0.5 or 1 day or a multiple of 1 day is due to the fact that we rarely have good coverage of the total phase for these periods. Moreover, these periods are mistaken for aliasing periods by the criterion we use to separate long- and short-term variables. For $P_{GCVS} > 10$ days and $P_{best} < 2$ days, the period-determination failure is due to persisting aliasing effects (and sometimes photometric errors). The P_{best} found is in general a 1 day divider.

We found the P_{GCVS} or $0.5P_{GCVS}$ periods ($\pm 0.1P_{GCVS}$) in $\sim 47\%$ of the cases (43% when ROTSE and ASAS variables are included). This gives the statistical efficiency of period determinations in TSVSC1. Note that unsuccessful period determinations are essentially due to a temporal sampling of TAROT observations not adapted to P_{GCVS}.

4.2. Type Identifications for Periodic Variables

A tentative classification was performed using only our FLC data. We used a simple method based on the period and the Fourier coefficients as computed in equation (12). Following Simon & Lee (1981) we defined A_k and ϕ_k as

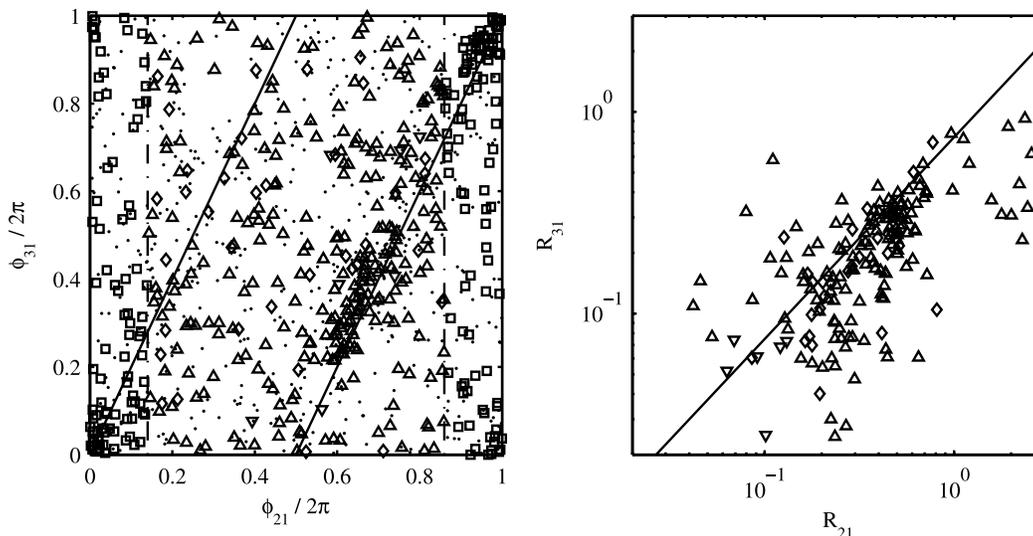$$A_k = \sqrt{a_k^2 + b_k^2}, \qquad \tan(\phi_k) = \frac{-b_k}{a_k}. \quad (13)$$

Fig. 6.—Classification of variable types. *Left*: Squares represent eclipsing binaries (EW and EAB). Dots represent long-period variables ($P > 50$ days). Upright and inverted triangles represent variables with $P < 1$ day, assumed to be RR Lyrae candidates (types AB and C, respectively). Diamonds represent variables with 1 day $< P < 50$ days and are assumed to be Cepheid candidates. Eclipsing binaries lie in the left and right margins ($\phi_{21}/2\pi < 0.14$ and $\phi_{21}/2\pi > 0.86$); RR Lyrae and Cepheid candidates lie near the diagonal lines (corresponding to smooth asymmetric light curves). *Right*: RR Lyrae C types (*inverted triangles*) lie in $R_{21} < 0.05$ and $R_{31} < 0.05$. For RR Lyrae AB (*upright triangles*) and Cepheid (*diamonds*) candidates, a fit gives $R_{32} = 0.75$.

Equation (12) can be rewritten as

$$m(i) = A_0 + \sum_{k=1}^{K} A_k \cos[2k\pi\varphi(i) + \phi_k]. \qquad (14)$$

We define

$$\phi_{k1} = \phi_k - k\phi_1, \qquad R_{ij} = A_i/A_j. \qquad (15)$$

The values of ϕ_{k1} are independent of the date chosen for the null phase and can be used to characterize the shape of the light curve.

Figure 6 describes the ranges used for our classification based on Klotz et al. (2007). The left panel shows that eclipsing stars have symmetrical light curves. They can be separated into contact, semidetatched, and detached classes as described in Pojmański (2002). RR Lyrae C stars have less deformed light curves than RR Lyrae AB stars and can also be distinguished by their shorter periods and lower amplitudes. Cepheids and RR Lyrae AB stars have similarly shaped light curves and are separated only by their periods. This classification is not to be relied on, because a good separation needs more data, such as color or spectral information. Table 2 summarizes the result of the classification.

5. THE TSVSC1 PUBLIC CATALOG

Between 2004 January and 2006 June, TAROT recorded 1.02×10^7 sources at least once in 1.78×10^5 images. TSVSC1 contains 1292 light curves corresponding to 1175 new variable stars observed in different cameras and filters. See Figure 7 for histograms of magnitudes and periods and Figure 8 for sample light curves.

Our selection only includes stars that verify a periodic or a long-term variation behavior, measured at least 30 times for long-period variables ($P > 20$ days) and at least 60 times for short-period ones. TSVSC1 stars are not present in either catalog listed in Table 3, nor in the AAVSO variable star index.[6] The period is given for each star, but it must be considered only as a best fit and not necessarily as the true period (see § 4.1.5). Public data of TSVSC1 can be downloaded from the CDS Web site[7] or in the tar package available in the electronic edition. TSVSC1 is made up of ASCII files that describe data and light-curve parameters for each star. The filename for a given star is coded as follows: [HTM area]-[star index]-[filter ASCII code]-[CAM index]. "HTM area" is

---

[6] See http://www.aavso.org/vsx.
[7] These data are also available online at http://tarot.obs-hp.fr/tsvsc1/.

TABLE 2
NUMBER OF TSVSC1 CANDIDATES IN EACH CLASS OF VARIABLE STAR

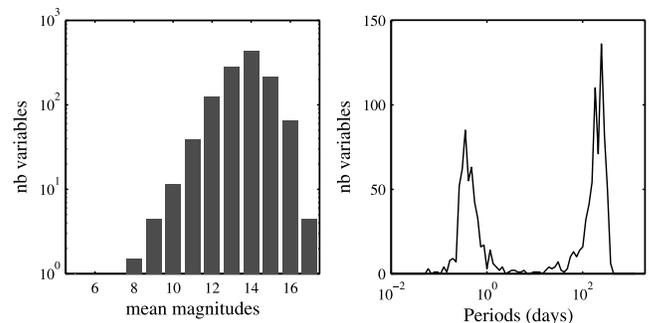| Variable Type	Number of Stars	Ratio (%)
Eclipsing Algol/β Lyrae....................	46	3.9
Eclipsing W Ursae Majoris	150	12.8
Other eclipsing.................................	5	0.4
RR Lyrae C..	7	0.6
RR Lyrae AB.....................................	282	24.0
Cepheid	40	3.4
Mira/semiregular...............................	645	54.9

Fig. 7.—*Left*: Histogram of mean magnitudes of 1175 variable stars. The completeness is at ~12.5 mag. *Right*: Histogram of periods.
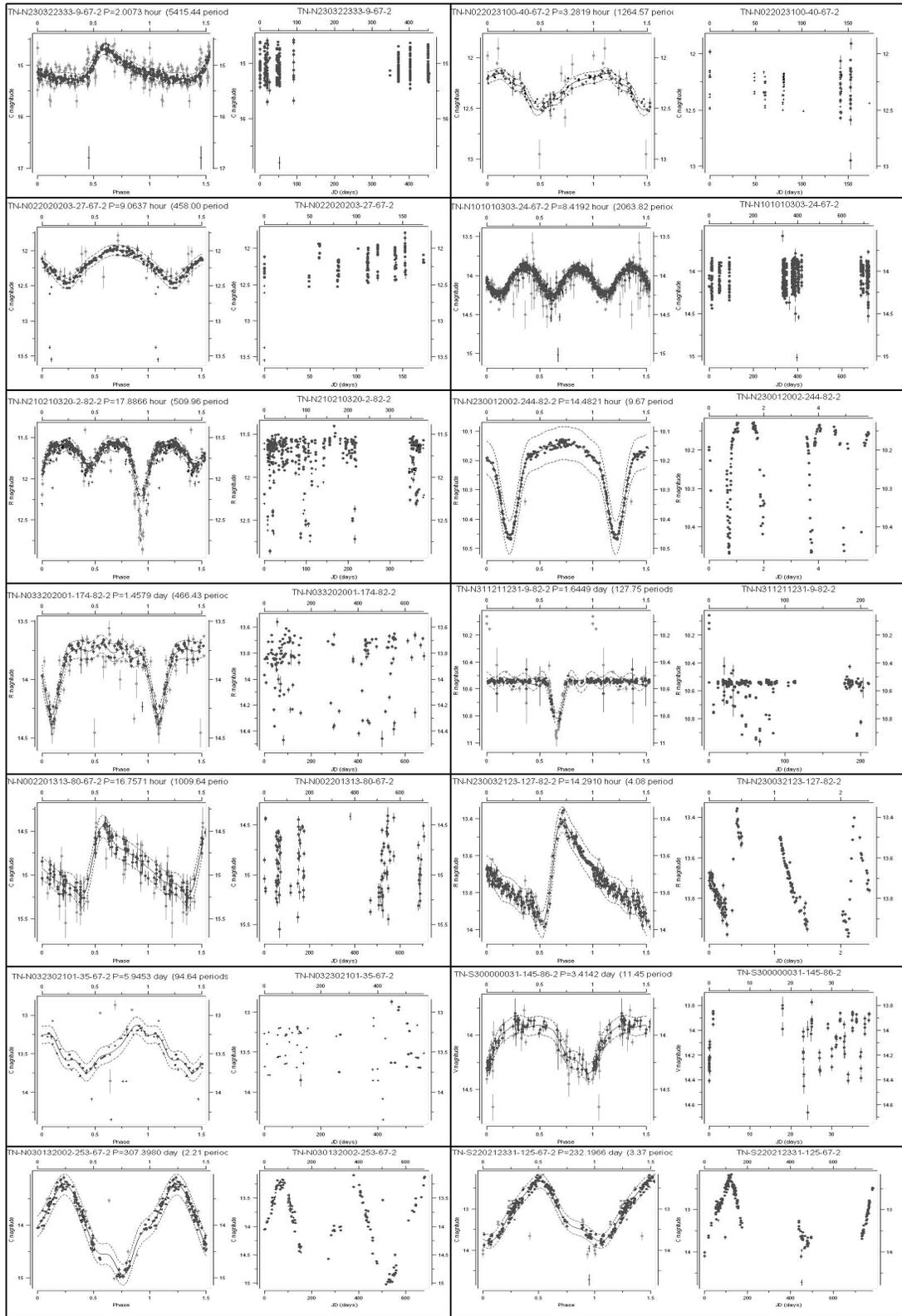
FIG. 8.—Sample of 14 TSVSC1 phased and nonphased light curves. [*See the electronic edition of the Journal for a color version of this figure.*]

TABLE 3
LIST OF CATALOGS USED FOR CROSS-IDENTIFICATIONS

CDS Catalog	Catalog Name	Flag
II/250	GCVS + NSV	1
J/AJ/128/2965	NSVS	2
J/A+A/399/365	ROTSE	2
J/AJ/119/1901	ROTSE	2
J/AJ/131/621	ROTSE	2
ACVS.1.1	ASAS	4
J/A+AS/112/407	OGLE	8
II/213	OGLE	8
J/A+AS/125/343	OGLE	8
J/other/AcA/48.289	OGLE	8
J/other/AcA/48.113	OGLE	8
J/other/AcA/49.223	OGLE	8
J/other/AcA/49.437	OGLE	8
J/other/AcA/49.543	OGLE	8
J/other/AcA/53.1	OGLE	8
J/MNRAS/349/1059	OGLE	8
J/MNRAS/353/705	OGLE	8
J/MNRAS/364/117	OGLE	8
J/A+A/439/559	OGLE	8
J/A+A/443/143	OGLE	8
J/A+AS/109/447	EROS	16
J/A+A/303/137	EROS	16
J/A+A/389/149	EROS	16
II/247	MACHO	32

NOTES.—Binary flags are used to separate GCVS 4.2, ROTSE, ASAS, EROS, MACHO, and OGLE catalogs. All catalogs are referenced to their CDS filename except for ACVS 1.1, which is available at http://archive.princeton.edu/~asas/. The ROTSE catalog is taken from Gettel et al. (2006).

described in § 3.1. "Star index" is the incremental index of this star in the HTM area. "Filter ASCII code" is the ASCII decimal code of the filter letter (e.g., $C = 67$, $V = 86$). "CAM index" is the index of the camera used for the corresponding measurements (CAM1 or CAM2, as described in § 2). The first lines of a TSVSC1 file are constituted by the header, ending with the word END. Each line of the header can be interpreted as a keyword followed by an equal sign and the corresponding value until the next carriage return. The useful information in the header is the TAROT designation, right ascension and declination (J2000.0), period, filter, barycentric Julian day of the zero phase, and Fourier coefficients described in equation (12). Data are stored in the next lines after the word END until the end of file. Each data line describes the UTC Julian Date, magnitude, magnitude 1 σ standard deviation, and the SExtractor quality flag. Note that the magnitude errors result from SExtractor photometry; we do not include differential photometry errors that can be approximated as systematic errors of about 0.05 mag. Observations continue with TAROT, and this first version of the TSVSC will be updated with the next year's results.

REFERENCES

Akerlof, C., et al. 1994, ApJ, 436, 787
Behrend, R., et al. 2006, A&A, 446, 1177
Bertin, E., & Arnouts, S. 1996, A&AS, 117, 393
Boër, M., et al. 2003, Messenger, 113, 45
Bringer, M., Boër, M., Peignot, C., Fontan, G., & Merce, C. 1999, A&AS, 138, 581
Cincotta, P. M., Mendez, M., & Nunez, J. A. 1995, ApJ, 449, 231
Eyer, L., & Bartholdi, P. 1999, A&AS, 135, 1
Gettel, S. J., Geske, M. T., & McKay, T. A. 2005, AJ, 131, 621
Klotz, A., Boër, M., Atteia, J. L., Stratta, G., Behrend, R., Malacrino, F., & Damerdji, Y. 2005, A&A, 439, L35
Klotz, A., Damerdji, Y., & Boër, M. 2007, in ASP Conf. Ser., Resolved Stellar Population, ed. D. Valls-Gabaud & M. Chavez (San Francisco: ASP), in press
Kunszt, P. Z., Szalay, A. S., & Thakar, A. R. 2001, in Mining the Sky, ed. A. J. Banday, S. Zaroubi, & M. Bartelmann (Heidelberg: Springer), 631

Lafler, M., & Kinman, A. 1965, ApJS, 11, 216
Larsson, S. 1996, A&AS, 117, 197
Le Borgne, J.-F., Klotz, A., & Boër, M. 2004, Inf. Bull. Variable Stars, 5568, 1
Pojmański, G. 2002, Acta Astron., 52, 397
Pravec, P., et al. 2003, IAU Circ., 8233, 3
Samus, N. N., et al. 2004, Combined General Catalog of Variable Stars (Moscow: Inst. Astron. Russian Acad. Sci. and Sternberg State Astron. Inst. Moscow State Univ.)
Scargle, J. D. 1982, ApJ, 263, 835
Simon, N. R., & Lee, A. S. 1981, ApJ, 248, 291
Stellingwerf, R. F. 1978, ApJ, 224, 953
Stetson, P. B. 1996, PASP, 108, 851
Udalski, A., et al. 1994, Acta Astron., 44, 165
Woźniak, P. R., et al. 2004, AJ, 127, 2436
Zwitter, T., Munari, U., & Moretti, S., 2004, IAU Circ., 8413, 1